AMERICAN SOCIETY FOR MICROBIOLOGY | mBio

Check for updates

| Environmental Microbiology | Research Article

# Methane production by *Methanothrix thermoacetophila* via direct interspecies electron transfer with *Geobacter metallireducens*

**Jinjie Zhou,**[1,2,3,4] **Jessica A. Smith,**[3,5] **Meng Li,**[1,4] **Dawn E. Holmes**[3,6]

**AUTHOR AFFILIATIONS** See affiliation list on p. 16.

**ABSTRACT** *Methanothrix* is widely distributed in natural and artificial anoxic environments and plays a major role in global methane emissions. It is one of only two genera that can form methane from acetate dismutation and through participation in direct interspecies electron transfer (DIET) with exoelectrogens. Although *Methanothrix* is a significant member of many methanogenic communities, little is known about its physiology. In this study, transcriptomics helped to identify potential routes of electron transfer during DIET between *Geobacter metallireducens* and *Methanothrix thermoacetophila*. Additions of magnetite to cultures significantly enhanced growth by acetoclastic methanogenesis and by DIET, while granular activated carbon (GAC) amendments impaired growth. Transcriptomics suggested that the OmaF-OmbF-OmcF porin complex and the octaheme outer membrane *c*-type cytochrome encoded by Gmet_0930, were important for electron transport across the outer membrane of *G. metallireducens* during DIET with *Mx. thermoacetophila*. Clear differences in the metabolism of *Mx. thermoacetophila* when grown via DIET or acetate dismutation were not apparent. However, genes coding for proteins involved in carbon fixation, the sheath fiber protein MspA, and a surface-associated quinoprotein, SqpA, were highly expressed in all conditions. Expression of gas vesicle genes was significantly lower in DIET- than acetate-grown cells, possibly to facilitate better contact between membrane-associated redox proteins during DIET. These studies reveal potential electron transfer mechanisms utilized by both *Geobacter* and *Methanothrix* during DIET and provide important insights into the physiology of *Methanothrix* in anoxic environments.

**IMPORTANCE** *Methanothrix* is a significant methane producer in a variety of methanogenic environments including soils and sediments as well as anaerobic digesters. Its abundance in these anoxic environments has mostly been attributed to its high affinity for acetate and its ability to grow by acetoclastic methanogenesis. However, *Methanothrix* species can also generate methane by directly accepting electrons from exoelectrogenic bacteria through direct interspecies electron transfer (DIET). Methane production through DIET is likely to further increase their contribution to methane production in natural and artificial environments. Therefore, acquiring a better understanding of DIET with *Methanothrix* will help shed light on ways to (i) minimize microbial methane production in natural terrestrial environments and (ii) maximize biogas formation by anaerobic digesters treating waste.

**KEYWORDS** *Methanothrix*, direct interspecies electron transfer (DIET), methane, magnetite, granular activated carbon (GAC), archaea, *Geobacter*, cytochromes, acetate

*Methanothrix* (formerly *Methanosaeta*) species, arguably the most prodigious methanogens on earth, substantially contribute to the production of atmospheric

**Editor** Terry C. Hazen, University of Tennessee at Knoxville, Knoxville, Tennessee, USA

Address correspondence to Meng Li, limeng848@szu.edu.cn.

See the funding table on p. 16.

**Received** 10 February 2023
**Accepted** 13 April 2023
**Published** 12 June 2023

methane and the conversion of wastes to methane biofuel (1). Species from this genus are frequently the most abundant methanogens in methanogenic terrestrial environments where soluble electron acceptors such as sulfate and nitrate are absent or negligible, for example, in natural wetlands and flooded rice paddy soils, as well as in many anaerobic digester systems (2–8). *Methanothrix* species are also important members of the methanogenic community in Arctic and Antarctic sediments (9–11), and scientists are particularly concerned with increases in methane production linked to melting permafrost in these polar terrestrial sediments as this will lead to a positive feedback loop that will further exacerbate climate change (12–14).

*Methanothrix* are one of only two methanogenic genera that can utilize acetate as a substrate for methanogenesis (1). Unlike the other acetoclastic methanogenic genus, *Methanosarcina*, *Methanothrix* have an extremely high affinity for acetate and generally maintain acetate at levels too low (μM range) for their competitors to metabolize (15). This ability to metabolize acetate at the low *in situ* levels found in most sediments and conventional mesophilic digesters is an important physiological capability, because acetate is a precursor for approximately two-thirds of the methane produced in terrestrial environments (1, 16) and is also an important intermediate in anaerobic digesters (17, 18).

Clearly, the importance of acetate as a methane precursor demonstrates the central role of *Methanothrix* in carbon and electron flow in many methanogenic environments. However, it has also been found that *Methanothrix* species can reduce $CO_2$ to methane by accepting electrons from exoelectrogenic bacteria via direct interspecies electron transfer (DIET) (4, 19), and this is likely to further increase their contribution to methane production in anoxic environments. Although *Methanothrix* species are predominant members of many methanogenic communities, little is known about their physiology (1, 20–23).

*Methanothrix* is considered a strictly acetoclastic methanogen; however, its genome contains genes from the $CO_2$ reduction pathway which is used by hydrogenotrophic methanogens for growth on $H_2/CO_2$ and formate (1). Studies of *Methanothrix harundinacea* growing in co-culture with *Geobacter metallireducens* showed that it could convert $^{14}C$-labelled $CO_2$ to $^{14}C$-methane, providing evidence that *Methanothrix* carries out $CO_2$ reduction during DIET (4). In addition, $CO_2$ reduction pathway genes were highly expressed by *Methanothrix* species growing by DIET in flooded rice paddy soils (2), anaerobic digesters treating waste (4, 24), and on the surface of cathodes in bioelectrochemical systems (25, 26). In a similar manner, acetoclastic *Methanosarcina* species growing by DIET with exoelectrogens highly expressed $CO_2$ reduction genes (27–29).

In addition to *Methanothrix*' high affinity for acetate (30), another feature that would make *Methanothrix* a strong competitor in low-nutrient environments is the ability to fix $CO_2$. All known *Methanothrix* species have genes coding for a RuBisCO-mediated reductive hexulose phosphate (RHP) pathway that forms formaldehyde as an intermediate (31, 32). They also have genes for a formaldehyde-activating enzyme (Fae), an enzyme that catalyzes the conversion of formaldehyde into 5,10-methylenetetrahydromethanopterin, an intermediate in the methanogenic $CO_2$ reduction pathway. Metatranscriptomic data demonstrated that *Methanothrix* was highly expressing genes from the RHP pathway in an anaerobic digester (31).

In order to further understand the physiology of DIET between an exoelectrogen and *Methanothrix*, co-cultures were established between *G. metallireducens* and *Methanothrix thermoacetophila*. Previous studies have shown that conductive materials can enhance DIET between exoelectrogens and methanogens (33–38), and they are frequently added to bioreactors dominated by *Methanothrix* species (24). Therefore, to more fully understand the impact that conductive materials can have on *Methanothrix* physiology, two different conductive materials, granular activated carbon (GAC) and magnetite nanoparticles were added to *Mx. thermoacetophila* cultures. Transcriptomic studies were also done to identify potential pathways for electron transfer between the electron-donating (*G. metallireducens*) and electron-accepting (*Mx. thermoacetophila*) partners.

These results provide valuable insights into *Methanothrix* physiology that can be used to better understand carbon flow in many methanogenic terrestrial ecosystems and to help optimize biomethane production from waste.

## RESULTS AND DISCUSSION

### *Mx. thermoacetophila* can accept electrons from *G. metallireducens* via DIET

Co-cultures of *G. metallireducens* and *Mx. thermoacetophila* were grown with ethanol (20 mM) provided as the sole electron donor, and $CO_2$ [supplied as a gas mixture of $N_2/CO_2$ (80/20 v/v) at atmospheric pressure] as the sole electron acceptor (Fig. 1). Neither of the partners would survive alone in this medium, as the bacterium lacked an electron acceptor, and the methanogen lacked an electron donor. Utilization of $H_2$/formate mediated electron transfer was also not possible because *G. metallireducens* does not produce $H_2$ or formate during ethanol oxidation (39, 40), and *Mx. thermoacetophila* cannot use $H_2$ or formate as an electron donor (41). Therefore, any methane produced by this co-culture resulted from DIET between *G. metallireducens* and *Mx. thermoacetophila*.

It took 95 days for initial co-culture aggregates to form, which is comparable to the time needed for co-cultures of *G. metallireducens* and *Methanothrix soehngenii* to become established (82 days), but much faster than co-cultures with *G. metallireducens* and *Mx. harundinacea* (167 days) (19) (Fig. S1). Once DIET was established, ethanol was converted to methane with a yield of 1.46 mol methane/mol ethanol in 15 days, and acetate concentrations initially increased until day 7 and then started to decline (Fig. 1). According to the stoichiometry of ethanol consumption and methane production (equations 1–4), two-thirds of the methane generated by the co-culture was produced by acetoclastic methanogenesis, and one-third was produced via DIET (4, 28, 35, 42).

$$\text{Ethanol oxidation by } \textit{Geobacter}: C_2H_6O + H_2O \rightarrow C_2H_4O_2 + 4H^+ + 4e^- \quad (1)$$

$$\text{Acetoclastic methanogenesis by } \textit{Methanothrix}: C_2H_4O_2 \rightarrow CO_2 + CH_4 \quad (2)$$

$$\text{DIET} - \text{based methanogenesis by } \textit{Methanothrix}: 4H^+ + 4e^- + 0.5CO_2 \rightarrow 0.5CH_4 + H_2O \quad (3)$$

$$\text{In sum}: C_2H_6O \rightarrow 1.5CH_4 + 0.5CO_2 \quad (4)$$

In addition, the rate of methane production was significantly faster than the rate of established co-cultures of *G. metallireducens* and *Mx. harundinacea* which took 85 days to reduce 20 mM ethanol to methane (4). This rate was comparable to co-cultures established with *G. metallireducens* and *Methanosarcina vacuolata* DH-1 (15 days) but was 1.9–2.3 times faster than rates seen in co-cultures with *G. metallireducens* and *Metha-*

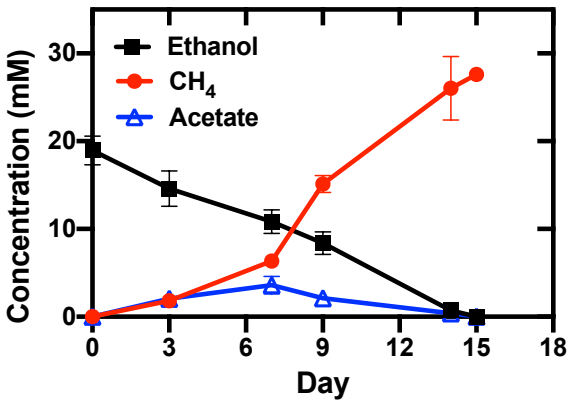


**FIG 1** Growth of *Geobacter metallireducens* and *Methanothrix thermoacetophila* co-cultures with ethanol (20 mM) provided as the sole electron donor and $CO_2$ provided as the sole electron acceptor. Data represent means and standard deviations from triplicate cultures.

*nosarcina barkeri* (~31 days), *Methanosarcina acetivorans* (28 days), or *Methanosarcina subterranea* (35 days) (28, 35, 42). *G. metallireducens* and *Mx. thermoacetophila* formed visibly large, loosely clumped aggregates (Fig. 2A), rather than the tight balls formed when *G. metallireducens* served as the electron-donating partner for DIET with other organisms (4, 40, 43). Confocal (Fig. 2B and C) and transmission electron microscopy (TEM) (Fig. 2D through G) images showed that *G. metallireducens* cells (short orange rods) were closely attached to the sheath of *Methanothrix* (green long filaments). Quantitative PCR of DNA extracted from these aggregates revealed that *G. metallireducens* accounted for over three quarters (76.03 ± 2.18%) of the cells, likely because one long fiber-like cell of *Methanothrix* served as a scaffold for the attachment of multiple *Geobacter* cells.

## Magnetite enhanced growth of *Mx. thermoacetophila,* while GAC had an inhibitory effect

Previous studies have shown that the addition of conductive materials, such as GAC (19, 38, 44) and magnetite (45), can stimulate DIET between *G. metallireducens* and an electron-accepting partner. GAC is a representative carbon-based material with a large surface area and high electrical conductivity. In contrast, nanoscale magnetite is a typical iron-based conductive material that is abundant in soils and sediments (46, 47). Therefore, co-cultures were grown in the presence of both of these materials.

It was surprising to find that growth of *Mx. thermoacetophila* alone or in co-culture with *G. metallireducens* was severely impaired by the presence of GAC (Fig. 3). In fact, acetoclastic methanogenesis was inhibited by GAC at concentrations above 20 g/L (Fig. 3A). In addition, DIET co-cultures could not become established in the presence of GAC (Fig. 3B; Fig. S1).

GAC is frequently added to anaerobic digesters to promote methane production (48, 49), and in many cases, the proportion of *Methanothrix* species declines while *Methanosarcina* species are enriched in GAC-amended reactors (50–53). The results from this study help explain why *Methanothrix* is often less abundant in GAC-amended reactors and indicate that GAC may not be the best option for stimulation of methanogenesis in environments where *Methanothrix* is an important member of the community. Further investigations into the inhibitory nature of GAC on the growth of *Methanothrix* are warranted.

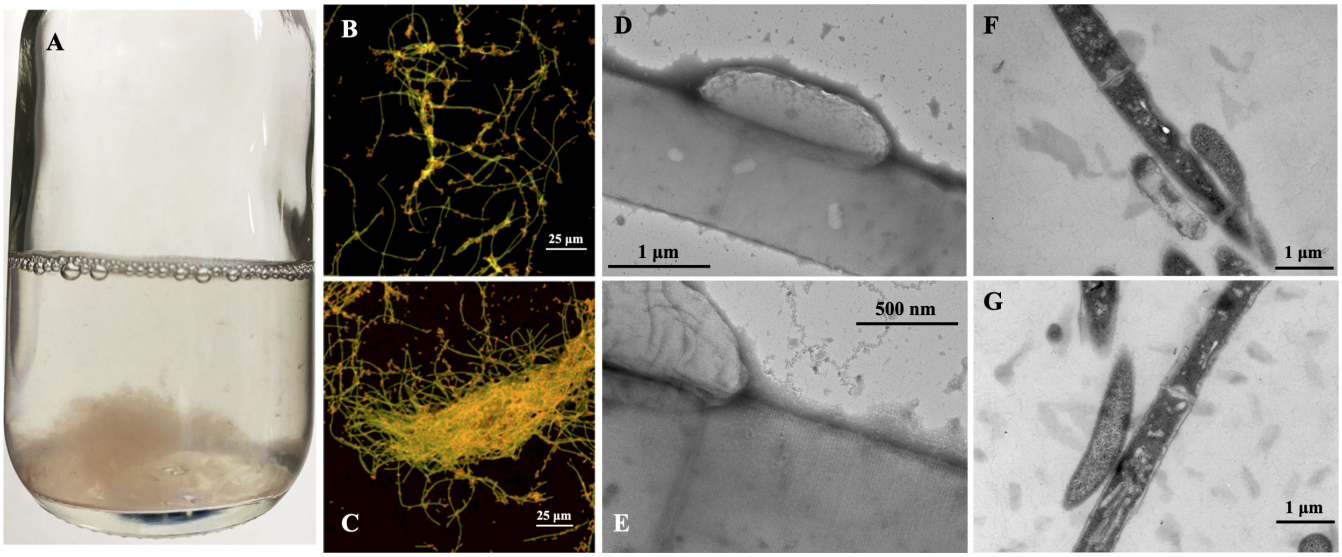


**FIG 2** Morphology of *Geobacter metallireducens* and *Methanothrix thermoacetophila* co-culture aggregates. (A) Appearance of loose aggregates visible to the naked eye; (B and C) FISH images showing the close attachment of *G. metallireducens* (short rod, orange) cells to *Mx. thermoacetophila* (long filament, green); (D and E) Negative-stain TEM images of co-cultures; (F and G) Ultrathin TEM images of co-cultures. FISH, fluorescence *in situ* hybridization; TEM, transmission electron microscopy.

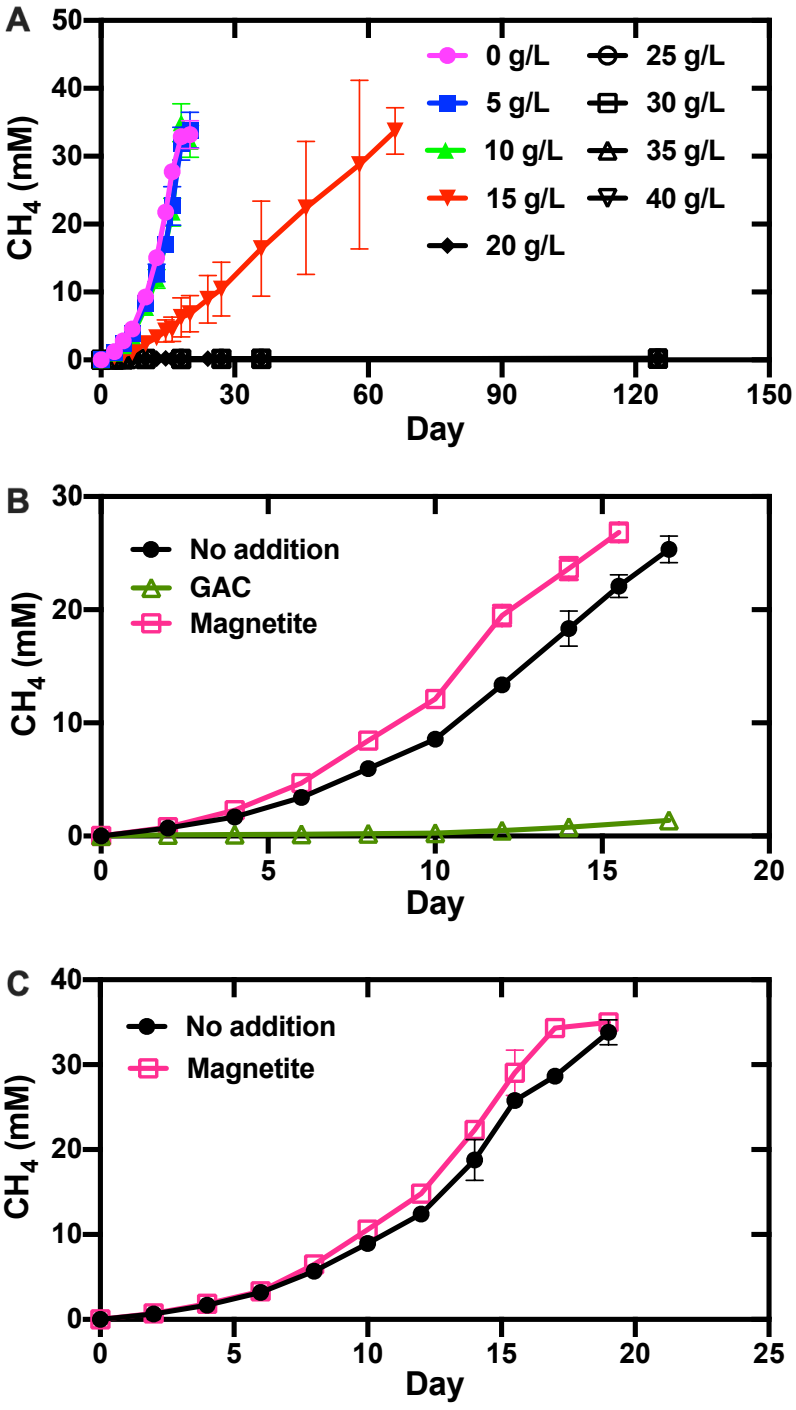


**FIG 3** Effects of granular activated carbon (GAC) and magnetite on methane production by *Methanothrix thermoacetophila*. (A) Pure cultures using acetate (40 mM) as substrate in the presence of various GAC concentrations; (B) co-cultures using ethanol (20 mM) as substrate in the presence of GAC (40 g/L) or magnetite (10 mM); (C) pure cultures using acetate (40 mM) as substrate in the presence of magnetite (10 mM). Data represent the average and standard deviations from triplicate cultures.

Similar to previous studies with *Methanosarcina* (54, 55), the addition of magnetite slightly stimulated (1.2 times faster; *P* value = 0.05) the rate of growth for pure cultures grown by acetoclastic methanogenesis (Fig. 3C). Growth in co-culture was also enhanced and aggregates only took 45 days to form compared to 95 days in nonamended

co-cultures (Fig. S1). Once aggregates became established, they grew at rates that were 1.2 times faster (*P* value = 0.007) (Fig. 3B). Consistent with these results, magnetite additions have also been shown to stimulate methanogenesis by *Methanothrix* species participating in DIET in anaerobic digesters (56) and by *Methanosarcina* growing with *Geobacter* in methanogenic rice paddy soil enrichments (57).

## The *G. metallireducens* DIET transcriptome

### *G. metallireducens transcriptomes are similar when cells are grown in co-culture with Mx. thermoacetophila or M. barkeri*

The *G. metallireducens* transcriptome during growth by DIET with *Mx. thermoacetophila* (MX) was compared to its DIET transcriptome when grown with other electron-accepting partners [*M. barkeri* (MB), *M. acetivorans* (MA), *M. subterranea* (MS), and *Geobacter sulfurreducens* (GS)] (58). Multidimensional scaling (MDS) analysis plots generated with the biological coefficient of variation (BCV) method (Fig. 4) revealed that the transcriptome of *G. metallireducens* grown in co-culture with *Mx. thermoacetophila* was most similar to its transcriptome when it was grown in co-culture with the type I *Methanosarcina* species, *M. barkeri* (42). Similar to *M. barkeri*, *Mx. thermoacetophila* lacks outer surface *c*-type cytochromes and does not have any potentially conductive archaella (28, 42). Transcriptomes from *G. metallireducens* cells grown by DIET with electron-accepting partners with cytochromes and potentially conductive e-pili/archaella (*G. sulfurreducens* and the type II *Methanosarcina* species *M. acetivorans* and *M. subterranea*) were significantly different.

## Genes from the PccF porin-cytochrome complex were more highly expressed in DIET-grown cells

Electron transport across the outer membrane of *Geobacter* cells to extracellular electron acceptors such as insoluble Fe(III) oxides or other microorganisms requires porin-*c*-type-cytochrome (Pcc) complexes (59, 60). *G. metallireducens* has three Pcc complexes; PccF (Gmet_0908-0910), PccG (Gmet_0911-0913), and PccH (Gmet_0825-0827) (58, 61). Similar to previous studies of DIET with *G. metallireducens* serving as the electron-donating partner (58), genes from the PccH complex were not highly expressed by *G. metallireducens* cells grown in co-culture with *Mx. thermoacetophila*. However, the number of transcripts from PccF complex genes, *omcF* (Gmet_0910), *omaF* (Gmet_0909), and *ombF* (Gmet_0908) were 6.0 (*P* value = $1.4 \times 10^{-11}$), 5.3 (*P* value = $7.2 \times 10^{-12}$), and 5.9 (*P* value = $4.1 \times 10^{-11}$) times more abundant in DIET-grown cells than Fe(III) respiring cells (Table 1; Table S1). Levels of transcripts from PccG complex genes, *omcG* (Gmet_0913), *omaG* (Gmet_0912), and *ombG* (Gmet_0911) were lower than the median RPKM values (Table S2) indicating that PccG was not important for DIET with *Mx. thermoacetophila*. Addition of magnetite to the *G. metallireducens*/*Mx. thermoacetophila* co-cultures increased the expression of PccG genes (Table 1), but the expression was still well below the median RPKM value (Table S2). This same pattern of increased expression of PccF relative to PccG genes was observed when *G. metallireducens* was grown in co-culture with *M. barkeri* (58).

## Pilin genes were not more highly expressed in DIET-grown cells

Although genes coding for PilA, the monomer of *Geobacter* e-pili (62), and Spc, the putative e-pili chaperone protein (63), were being expressed by DIET-grown cells at levels >3.5 times above the median RPKM values (Table S2), significant differences in expression were not observed between DIET- and Fe(III)-respiring cells (Table 1). These results suggest that e-pili may not be as important for DIET with *Mx. thermoacetophila* as they are for DIET with *M. acetivorans* and *G. sulfurreducens*, both of which required e-pili for DIET-based growth and expressed *pilA* and *spc* genes at levels that were >two fold higher in DIET-grown cells than Fe(III)-respiring cells (28, 39). Other electron-accepting species lacking *c*-type cytochromes, *M. barkeri* and *Methanobacterium electrotrophus* do

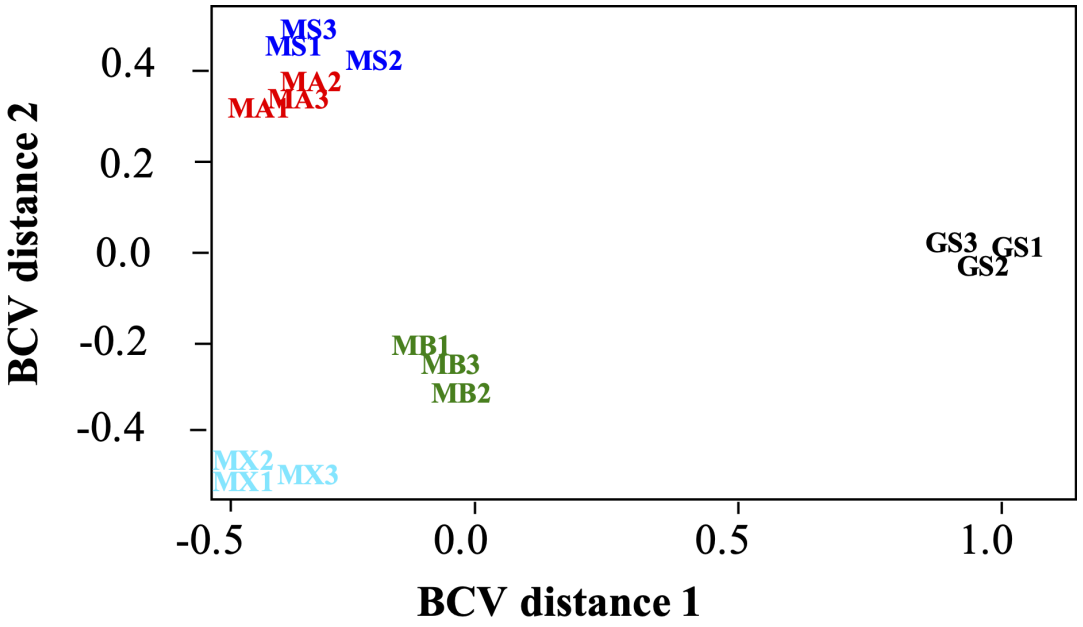


**FIG 4** Comparison of *Geobacter metallireducens* RNAseq libraries from co-cultures with *Methanothrix thermoacetophila* (MX), *Methanosarcina barkeri* (MB), *Methanosarcina acetivorans* (MA), *Methanosarcina subterranea* (MS), and *Geobacter sulfurreducens* (GS) using multidimensional scaling analysis with the biological coefficient of variation (BCV) method.

not require e-pili for DIET (37, 58, 64). Therefore, *Mx. thermoacetophila* may be another electron-accepting partner lacking outer surface *c*-type cytochromes that does not require e-pili for participation in DIET. However, further studies with gene deletion strains are required.

It was also interesting to find that the addition of magnetite to the co-cultures decreased the expression of e-pili associated genes; *pilA* (Gmet_1399) and *spc* (Gmet_1400) transcripts were 3.0 (*P* value = $2.3 \times 10^{-9}$) and 4.3 (*P* value = $8.6 \times 10^{-11}$) times less abundant in DIET co-cultures amended with magnetite (Table 1; Table S1). Studies have indicated that magnetite can compensate for pilin-associated *c*-type cytochromes involved in extracellular electron exchange during DIET between *Geobacter* species (45, 65).

## Genes coding for Gmet_0930 and the CbcABCDE complex were highly expressed by DIET-grown cells

Genes coding for two periplasmic multiheme *c*-type cytochromes (Gmet_2928 and Gmet_0534) and an outer surface multiheme *c*-type cytochrome (Gmet_0930) were >20 times more highly expressed by *G. metallireducens* cells grown by DIET with *Mx. thermoacetophila* than Fe(III)-respiring cells (Table 1). Gmet_2928 codes for CbcA, a periplasmic 7-heme cytochrome that is part of the cytochrome *bc* complex CbcABCDE (Gmet_2928-2932). Cytochrome *bc* (Cbc) complexes are composed of a transmembrane *b*-type cytochrome in close association with at least one multiheme *c*-type cytochrome, and they are involved in shuttling electrons from the quinone pool in the inner membrane to *c*-type cytochromes found in the periplasmic space (60, 66, 67). The gene coding for CbcA and other components of this complex, the *b*-type cytochrome (CbcB), two other periplasmic *c*-type cytochromes (CbcC and CbcD), and a membrane protein (CbcE), were 28.9 (*P* value = $2.0 \times 10^{-14}$), 41.7 (*P* value = $5.7 \times 10^{-14}$), 2.6 (*P* value = $2.2 \times 10^{-6}$), 2.0 (*P* value = $2.1 \times 10^{-6}$), and 2.8 (*P* value = $1.5 \times 10^{-8}$) times more highly expressed in DIET-grown cells than Fe(III)-respiring cells (Table 1; Table S1).

Gmet_0534 codes for a 5-heme periplasmic cytochrome putatively associated with another Cbc complex, CbcMNOPQR (Gmet_0533–0539). Although this gene was 28.2

**TABLE 1** Differences in expression of genes coding for electron transfer proteins in *Geobacter metallireducens* cells grown under various conditions[a]

| Locus ID | Annotation | Gene | Location | DIET vs Fe(III)-citrate | DIET- magnetite vs DIET | DIET vs DIET-magnetite |
|---|---|---|---|---|---|---|
| Gmet_0910 | 10 heme *c*-type cytochrome from PccF complex | *omcF* | Outer membrane/surface | 6.00 | 2.96 | NS |
| Gmet_0909 | 9 heme periplasmic *c*-type cytochrome from PccF complex | *omaF* | Periplasmic | 5.32 | 2.76 | NS |
| Gmet_0908 | Porin protein from the PccF complex | *ombF* | Outer membrane/surface | 5.88 | 2.11 | NS |
| Gmet_0913 | 9 heme outer membrane *c*-type cytochrome from PccG | *omcG* | Outer membrane/surface | NS | 2.78 | NS |
| Gmet_0912 | 8 heme periplasmic *c*-type cytochrome from PccG complex | *omaG* | Periplasmic | NS | 4.79 | NS |
| Gmet_0911 | Porin protein from the PccG complex | *ombG* | Outer membrane/surface | NS | 3.64 | NS |
| Gmet_1399 | Type IV major pilin subunit, PilA | *pilA* | Outer membrane/surface | NS | NS | 2.96 |
| Gmet_1400 | Short pilin chaperone protein, Spc | *spc* | Outer membrane/surface | NS | NS | 4.29 |
| Gmet_2928 | 7 heme *c*-type cytochrome protein from CbcABCDE | *cbcA* | Periplasmic | 28.86 | NS | NS |
| Gmet_2929 | *b*-type cytochrome from CbcABCDE complex | *cbcB* | Inner membrane | 41.70 | NS | NS |
| Gmet_2930 | Cytochrome c family protein, 11 hemes | *cbcC* | Periplasmic | 2.55 | NS | NS |
| Gmet_2931 | Monoheme *c*-type cytochrome protein from CbcABCDE complex | *cbcD* | Periplasmic | 2.00 | NS | NS |
| Gmet_2932 | Membrane protein from CbcABCDE complex | *cbcE* | Inner membrane | 2.80 | 2.35 | NS |
| Gmet_0533 | Membrane protein from CbcMNOPQR | *cbcQ* | Inner membrane | 51.56 | NS | NS |
| Gmet_0534 | *c*-type cytochrome protein, 5 hemes | *cbcR* | Periplasmic | 28.19 | NS | NS |
| Gmet_0930 | *c*-type cytochrome, 8 hemes | | Outer membrane/surface | 20.45 | NS | NS |
| Gmet_1210 | *c*-type cytochrome, 2 hemes | *ccpB* | Periplasmic | 5.95 | NS | NS |
| Gmet_0252 | Monoheme *c*-type cytochrome protein | *coxB* | Inner membrane | 4.53 | NS | NS |
| Gmet_1809 | *c*-type cytochrome, 5 hemes | *actA* | Inner membrane | 3.98 | NS | NS |
| Gmet_1019 | *c*-type cytochrome, 2 hemes | *narC* | Inner membrane | 3.81 | NS | NS |
| Gmet_2626 | Monoheme P460 *c*-type cytochrome | | Unknown | 3.37 | NS | NS |
| Gmet_0294 | *c*-type cytochrome, 4 hemes | *nrfA* | Periplasmic | 3.14 | NS | NS |
| Gmet_3091 | *c*-type cytochrome protein, 2 hemes | *macA* | Periplasmic | 3.07 | 2.69 | NS |
| Gmet_0679 | *c*-type cytochrome, 5 hemes | | Unknown | 2.84 | NS | NS |
| Gmet_1197 | *c*-type cytochrome, 5 hemes | | Unknown | 2.71 | 3.14 | NS |
| Gmet_0142 | *c*-type cytochrome, 8 hemes | | Periplasmic | 2.44 | NS | NS |
| Gmet_1814 | Monoheme *c*-type cytochrome | *actE* | Unknown | 2.30 | NS | NS |
| Gmet_0292 | Diheme *c*-type cytochrome | | Outer membrane/surface | 2.08 | NS | NS |
| Gmet_1647 | Diheme *c*-type cytochrome | | Unknown | 2.07 | NS | NS |
| Gmet_0558 | *c*-type cytochrome protein, 27 hemes | *omcO* | Unknown | NS | 10.62 | NS |
| Gmet_1087 | Monoheme *c*-type cytochrome | | Unknown | NS | 7.19 | NS |
| Gmet_0571 | *c*-type cytochrome protein, 34 hemes | | Outer membrane/surface | NS | 3.23 | NS |
| Gmet_0121 | Diheme *c*-type cytochrome | | Unknown | NS | 2.89 | NS |
| Gmet_2896 | *c*-type cytochrome protein, 4 hemes | | Outer membrane/surface | NS | 2.79 | NS |
| Gmet_0600 | *c*-type cytochrome protein, 19 hemes | | Outer membrane/surface | NS | 2.67 | NS |
| Gmet_2839 | *c*-type cytochrome protein, 11 hemes | | Periplasmic | NS | 2.65 | NS |

(*Continued on next page*)

**TABLE 1** Differences in expression of genes coding for electron transfer proteins in cells grown under various conditions (*Continued*)

| Locus ID | Annotation | Gene | Location | DIET vs Fe(III)-citrate | DIET- magnetite vs DIET | DIET vs DIET-magnetite |
|---|---|---|---|---|---|---|
| Gmet_1094 | Diheme *c*-type cytochrome | *cccA* | Unknown | NS | 2.45 | NS |
| Gmet_0330 | Monoheme *c*-type cytochrome | *narH* | Inner membrane | NS | 2.36 | NS |
| Gmet_0557 | *c*-type cytochrome protein, 4 hemes | | Unknown | NS | 2.25 | NS |
| Gmet_0598 | *c*-type cytochrome protein, 22 hemes | | Outer membrane/surface | NS | 2.15 | NS |
| Gmet_1846 | Diheme *c*-type cytochrome | *ppcE* | Periplasmic | NS | NS | 3.06 |
| Gmet_2902 | Diheme *c*-type cytochrome | *ppcA* | Periplasmic | NS | NS | 4.08 |
| Gmet_3166 | Diheme *c*-type cytochrome | *ppcB* | Periplasmic | NS | NS | 2.75 |
| Gmet_1867 | *c*-type cytochrome protein, 8 hemes | | Unknown | NS | NS | 2.45 |
| Gmet_2432 | Monoheme P460 *c*-type cytochrome | | Unknown | NS | NS | 5.57 |

[a]Values represent fold differences between *G. metallireducens* cells grown by DIET with *Methanothrix thermoacetophila* compared to growth with ethanol (20 mM) as the electron donor and ferric citrate (56 mM) as the electron acceptor (DIET vs Fe(III)-citrate); *G. metallireducens* cells grown by DIET with *Mx. thermoacetophila* in the presence of 10 mM magnetite versus DIET without magnetite (DIET-magnetite vs DIET); or *G. metallireducens* cells grown by DIET with *Mx. thermoacetophila* without magnetite compared to DIET with magnetite (DIET vs DIET-magnetite). Only genes with fold differences >2 and *P* values <0.05 were considered significant. NS: no significant difference. *P* values are available in Table S1.

times (*P* value = $3.5 \times 10^{-14}$) more highly expressed in DIET-grown cells, *cbcQ* was the only other gene from this complex that was more highly expressed by DIET-grown cells (Table 1; Table S1). Genes from both the CbcABCDE and CbcMNOPQR complexes were highly expressed by *G. metallireducens* cells grown by DIET with other electron-accepting partners and during growth with insoluble Fe(III) oxide; however, genetic studies showed that they were not required for growth in either of these conditions (58, 68).

Gmet_0930 encodes an 8-heme outer surface *c*-type cytochrome that was 20.4 (*P* value = $7.5 \times 10^{-14}$) times more highly expressed by DIET-grown than Fe(III)-respiring cells (Table 1; Table S1). *G. metallireducens* requires this *c*-type cytochrome for formation of DIET aggregates with *G. sulfurreducens* (58) and it was among the most highly expressed genes by *G. metallireducens* cells grown in co-culture with *M. acetivorans*, *M. subterranea*, and *M. barkeri*. Although Gmet_0930 deletion mutant strains eventually adapted to grow in co-culture with all three *Methanosarcina* species, growth was impaired even after four transfers indicating that Gmet_0930 was also important for DIET with these other partners (58).

Significant differences in expression of the periplasmic cytochrome PpcA (Gmet_2902) were not observed between DIET grown and Fe(III)-respiring cells. However, PpcA (Gmet_2902) was the second most highly expressed *c*-type cytochrome with values that were 21 times higher (*P* values = $3.2 \times 10^{-5}$) than median RPKM values for both DIET and DIET-magnetite conditions (Table S2). PpcA is highly conserved among *Geobacter* species and it is required for optimal Fe(III) reduction by *G. sulfurreducens* (69, 70). Based on analysis of transcriptomic data, it is proposed that the route for electron transfer from the quinone pool in the *G. metallireducens* inner membrane to *Mx. thermoacetophila* during DIET requires activity from the CbcABCDE complex, periplasmic PpcA, the PccF conduit (*omaF*, *ombF*, and *omcF*), and the outer surface *c*-type cytochrome Gmet_0930 (Fig. 5).

## The *Mx. thermoacetophila* DIET transcriptome

Unfortunately, analysis of transcriptomic data did not reveal any significant differences between DIET-based and acetoclastic metabolism in *Mx. thermoacetophila*. In all of the conditions, most genes from pathways for methanogenesis from acetate and $CO_2$, carbon fixation, the reductive citric acid cycle, and carbon monoxide and formate metabolism had RPKM values that were more than two-fold above median RPKM values (Supplementary text; Fig. 6; Table S3). Many of these genes were also more highly expressed under both acetoclastic and DIET-based conditions in the presence of magnetite.

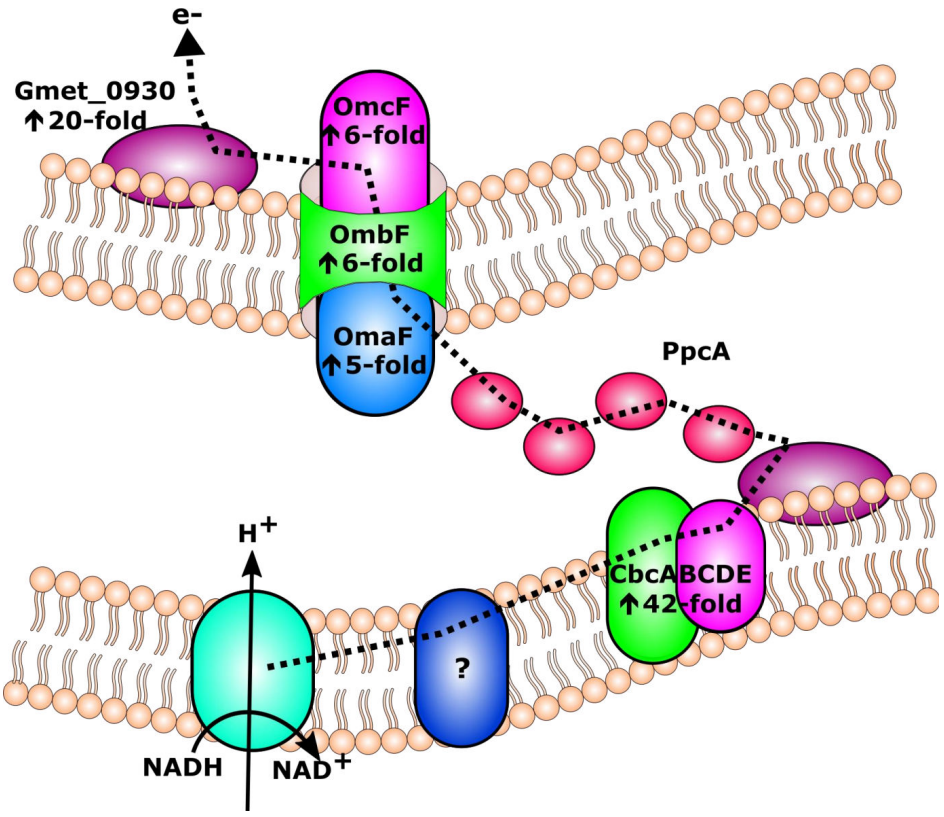


**FIG 5** Proposed pathway for electron transfer in *Geobacter metallireducens* during DIET with *Methanothrix thermoacetophila*. Electrons are transferred from the quinone pool in the inner membrane to the CbcABCDE quinone-oxidoreductase complex, then to the periplasmic *c*-type cytochrome PpcA, which then shuttles electrons to the PccF (OmaF, OmbF, and OmcF) porin-cytochrome complex and then to the outer surface octaheme cytochrome encoded by Gmet_0930. Electrons may then be transferred directly to *Mx. thermoacetophila*. Arrows represent fold upregulated in DIET grown cells compared to cells grown with ethanol as the electron donor and ferric citrate as the electron acceptor (for proteins composed of multiple subunits, values from the most highly expressed subunits are shown). If an arrow is not listed with a protein from the proposed pathway, the gene was not differentially expressed between DIET- and Fe(III)-respiring cells. DIET, direct interspecies electron transfer.

More specifically, comparison of DIET- to acetate-grown cells revealed that genes from the $CO_2$ reduction and the RHP carbon fixation pathways were being highly expressed by cells in both conditions. Previous studies have suggested that these genes are only highly expressed by DIET-grown *Methanothrix* cells (2, 4, 25, 31). However, transcriptomic comparisons between DIET-grown and acetoclastic cells were not done in these experiments.

The only clear differences in expression patterns between DIET- and acetate-grown cells were related to genes coding for gas vesicle proteins. Two gas vesicle gene clusters (Mthe_0055-0063 and Mthe_0069-0073) were >2 times (*P* value <0.05) more highly expressed in acetate-grown cells than DIET-grown cells in the presence and absence of magnetite (Table 2). Gas vesicles are commonly found in archaeal sheaths, including those from *Mx. thermoacetophila*, and make cells more buoyant within a water column (71, 72). This decrease in expression of gas vesicles during DIET may facilitate better contact between redox proteins on the surface of *G. metallireducens* and *Mx. thermoacetophila*.

Expression of *gvp* genes was also lower in DIET- and acetate-cells grown in the presence of magnetite. When the medium was supplemented with 10 mM magnetite, *Mx. thermoacetophila* sheaths were coated with magnetite particles (Fig. S2). It is possible that cells do not need to produce as many gas vesicles in the presence of magnetite

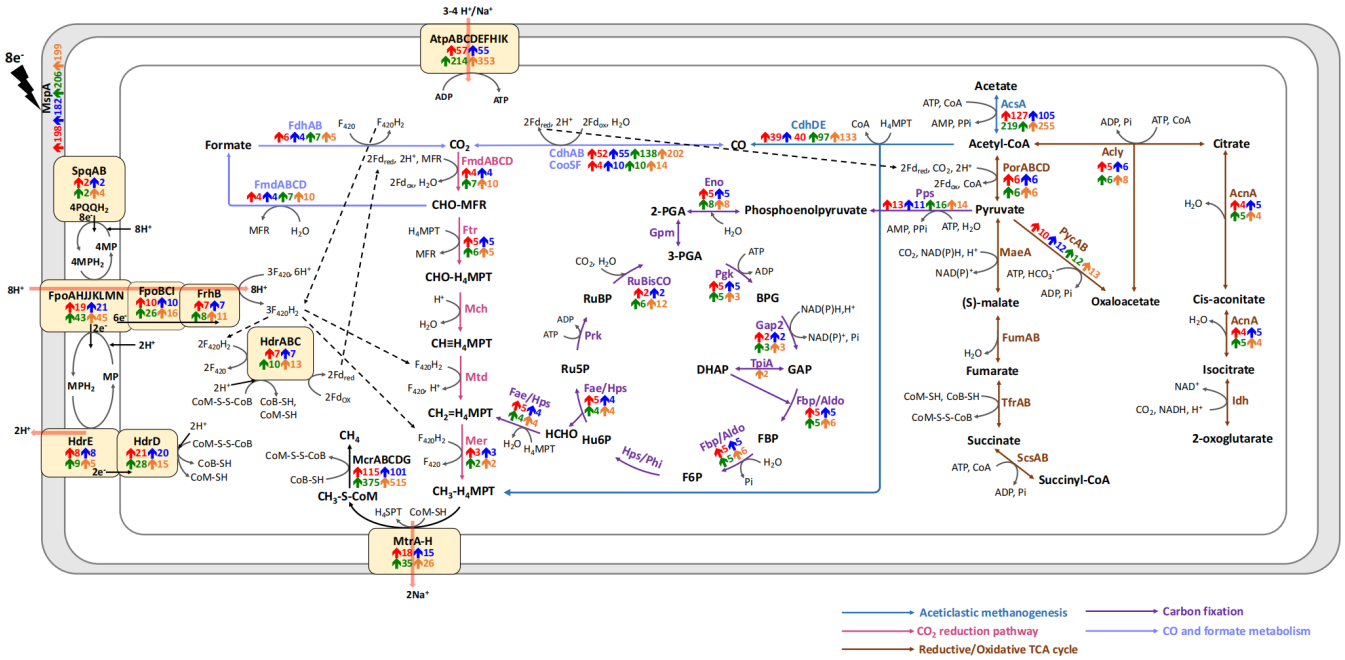


**FIG 6** Proposed pathways used by *Methanothrix thermoacetophila* during growth by acetoclastic and DIET-based methanogenesis in the presence or absence of magnetite. Arrows represent fold increase from median RPKM values (*P* values < 0.05) under DIET (red), acetate (blue), DIET+magnetite (green), and acetate+magnetite (orange) conditions. If proteins are composed of multiple subunits, values from the most highly expressed subunit are represented. Details regarding the fold differences and *P* values of each gene are provided in Table S3. CHO-MFR: formylmethanofuran; CHO-$H_4$MPT: formyltetrahydromethanopterin; CH≡$H_4$MPT: methenyltetrahydromethanopterin; $CH_2$=$H_4$MPT: methylenetetrahydromethanopterin; $CH_3$-$H_4$MPT: methyltetrahydromethanopterin; $CH_3$-S-CoM: 2-(methylthio)ethanesulfonate; Acetyl-CoA: acetyl-coenzyme A; 2-PGA: 2-phosphoglycerate; 3-PGA: 3-phosphoglycerate; BPG: 1,3-diphosphoglycerate; GAP: glyceraldehyde-3-phosphate; DHAP: dihydroxyacetone phosphate; FBP: fructose 1,6-bisphosphate; F6P: fructose 6-phosphate; Hu6P: D-arabino-3-hexulose-6-phosphate; Ru5P: ribulose-5-phosphate; HCHO: formaldehyde; RuBP: ribulose-1,5-bisphosphate; MP/$MPH_2$: oxidized/reduced forms of methanophenazine. DIET, direct interspecies electron transfer.

for several reasons: (i) magnetite can act as an electron conductor during DIET, (ii) the magnetite particles can serve as a scaffold for biofilm formation during DIET or acetoclastic growth, and (iii) acetate can adsorb to the positively charged magnetite particles reducing the need for cells to maintain buoyancy in the medium. Although transcriptomic data suggest that reduced expression of Gvp proteins is advantageous for DIET or growth in the presence of magnetite, differences in gas vesicle abundance were not obvious in negative-stain and ultrathin TEM images (data not shown).

## Possible routes for electron uptake by *Mx. thermoacetophila*

As discussed above, there were clear differences in expression of many genes in the presence or absence of magnetite (Table S4). However, these differences were not apparent in genes coding for surface-associated proteins that could potentially facilitate direct electron uptake from *G. metallireducens* (Table 3). This suggests that these genes may not be differentially regulated when cells are grown under varying conditions. Analysis of the most highly expressed surface proteins led us to the following proposed routes for electron uptake into *Mx. thermoacetophila*. However, this analysis is still speculative.

The main sheath fiber protein (MspA; Mthe_1069) was the most highly expressed surface-associated gene in all of the conditions and had >181 times (*P* values <1.14 × $10^{-5}$) higher expression than median RPKM values (Table 3; Fig. 6; Table S3). The MspA sheath protein forms amyloid fibrils with extended beta-sheet structures (71) and numerous aromatic amino acid residues (10.7% of the protein residues; Fig. S3). Previous studies have shown that stacked aromatic amino acids in amyloid fibrils confer

**TABLE 2** Differences in expression of genes coding for gas vesicle proteins in *Methanothrix thermoacetophila* cells grown under various conditions[a]

| Locus ID | Annotation | Gene | Acetate vs DIET | Acetate-magnetite vs DIET-magnetite | DIET vs DIET-magnetite | Acetate vs acetate-magnetite |
|---|---|---|---|---|---|---|
| Mthe_0055 | Gas vesicle synthesis GvpLGvpF fusion | *gvpLF* | 2.19 | 1.72 | 2.62 | 3.34 |
| Mthe_0056 | Gas vesicle protein GvpO | *gvpO* | 2.19 | 1.79 | 1.96 | 2.46 |
| Mthe_0058 | Gas vesicle protein GvpN | *gvpN* | 2.27 | 2.05 | 1.71 | 1.88 |
| Mthe_0060 | Gas vesicle synthesis protein GvpA | *gvpA* | 2.68 | 2.17 | 3.96 | 5.48 |
| Mthe_0061 | Gas vesicle synthesis protein GvpA | *gvpA* | 2.63 | 2.17 | 4.12 | 5.02 |
| Mthe_0062 | Gas vesicle synthesis protein GvpA | *gvpA* | 2.63 | 2.17 | 4.12 | 5.02 |
| Mthe_0063 | Gas vesicle synthesis protein GvpA | *gvpA* | 2.63 | 2.17 | 4.12 | 5.02 |
| Mthe_0069 | Gas vesicle protein GvpG | *gvpG* | 2.94 | NS | 4.53 | 11.07 |
| Mthe_0070 | Gas vesicle protein GvpA | *gvpA* | 2.89 | NS | 1.94 | 6.25 |
| Mthe_0071 | Gas vesicle protein GvpA | *gvpM* | 2.63 | NS | 2.82 | 8.85 |
| Mthe_0072 | Gas vesicle protein GvpK | *gvpK* | 2.69 | NS | 2.40 | 5.71 |
| Mthe_0073 | Gas vesicle synthesis GvpLGvpF fusion | *gvpLF* | 2.47 | NS | 2.06 | 4.72 |

[a]Values represent fold differences between *Mx. thermoacetophila* cells grown by acetoclastic methanogenesis versus cells grown by DIET with *Geobacter metallireducens* (acetate vs DIET) as well as in the presence of 10 mM magnetite (acetate-magnetite vs DIET magnetite); *Mx. thermoacetophila* cells grown by DIET with *G. metallireducens* without magnetite compared to DIET with magnetite (DIET vs DIET-magnetite); *Mx. thermoacetophila* cells grown by acetoclastic methanogenesis compared to acetoclastic methanogenesis with magnetite (acetate vs. acetate-magnetite). NS, no significant difference. All *P* values <0.05 and are available in Table S4. DIET, direct interspecies electron transfer.

conductivity (73), suggesting that MspA could be conductive. Thus, the surface-associated MspA sheath fiber protein of *Mx. thermoacetophila* may facilitate direct electron uptake from *G. metallireducens*.

Unlike *Geobacter* or type II *Methanosarcina* species (42, 60, 74, 75), *Mx. thermoacetophila* does not have any surface multiheme *c*-type cytochromes that could readily accept electrons from an extracellular electron donor (1, 76). However, the genome does have a gene coding for a transmembrane pyrroloquinoline quinone (PQQ) binding protein; surface quinoprotein A (*sqpA*; Mthe_0878) that was highly expressed (Table 3). The PQQ binding site of quinoproteins has a beta-propeller fold composed of antiparallel β-sheets radially arranged around a central tunnel (77, 78). The mature SqpA protein has an extremely high concentration of aromatic amino acids (11.3%) (Fig. S3), and pi stacking of aromatic residues arranged in the center of the funnel-shaped propeller could enhance electron transfer properties of this redox protein. Evidence that surface quinoproteins could be involved in DIET comes from observations that *M. barkeri*

**TABLE 3** Fold differences from median RPKM values for *Methanothrix thermoacetophila* genes coding for surface proteins that could potentially facilitate electron uptake from *Geobacter metallireducens* in all four conditions[a]

| Locus ID | Annotation | Gene | DIET | Acetate | DIET-magnetite | Acetate-magnetite |
|---|---|---|---|---|---|---|
| Mthe_0878 | Surface pyrroquinoline quinone (PQQ) protein | *sqpA* | 2.18 | 2.18 | 2.27 | 3.55 |
| Mthe_0322 | Cell surface protein with copper binding domain | | 3.97 | 4.48 | 4.73 | 3.54 |
| Mthe_0787 | Cell surface protein with copper binding domain | | 5.42 | 4.55 | 4.50 | 5.08 |
| Mthe_1273 | Cell surface protein with copper binding domain | | 2.95 | 3.27 | 3.33 | 3.78 |
| Mthe_1510 | Cell surface protein with copper binding domain | | 1.67 | 2.42 | 2.21 | 4.12 |
| Mthe_0046 | Cell surface protein with copper binding domain | | 4.06 | 4.21 | 3.33 | 4.70 |
| Mthe_1626 | Cell surface protein with copper binding domain | | 4.32 | 5.44 | 5.81 | 11.72 |
| Mthe_1069 | Major sheath protein | *mspA* | 198.15 | 181.98 | 205.78 | 198.57 |
| Mthe_1070 | Major sheath protein | | 13.66 | 15.11 | 22.23 | 30.17 |
| Mthe_0677 | S-layer-related duplication domain | | 303.63 | 319.81 | 316.80 | 392.27 |
| Mthe_0149 | S-layer-related duplication domain | | 17.52 | 18.48 | 20.41 | 30.20 |
| Mthe_1177 | S-layer-related duplication domain | | 4.13 | 4.35 | 4.67 | 5.06 |

[a]DIET: *Mx. thermoacetophila* cells grown in co-culture with *G. metallireducens* with ethanol (20 mM) as the electron donor (median $\log_2$ RPKM value was 7.31), Acetate: *Mx. thermoacetophila* grown with acetate (40 mM) (median $\log_2$ RPKM value was 7.30), DIET-magnetite: DIET with *Mx. thermoacetophila* and *G. metallireducens* with ethanol (20 mM) as the electron donor in the presence of magnetite (10 mM) (median $\log_2$ RPKM value was 7.29), Acetate-magnetite: *Mx. thermoacetophila* grown with acetate (40 mM) in the presence of magnetite (10 mM) (median $\log_2$ RPKM value was 7.27). All *P* values are <0.05 and were calculated by ANOVA using the R statistical package. *P* values are available in Table S3.

was expressing genes encoding surface quinoproteins during growth via DIET with *G. metallireducens* (27) and *Rhodopseudomonas palustris* (29).

It is possible that electrons accepted by a membrane-associated electron carrier such as SqpA are being funneled to Fpo dehydrogenase to reduce $F_{420}$ or ferredoxin in a manner similar to that suggested by *Methanosarcina* (Fig. 6) (27–29). Unlike *mspA* and *sqpA*, Fpo dehydrogenase genes were differentially expressed in cells grown in the presence of magnetite (Table S4). In addition, elucidation of the role that Fpo dehydrogenase might play in DIET is further complicated by the fact that it is also likely to be involved in acetoclastic methanogenesis (21). The Fpo dehydrogenase complex of *Mx. thermoacetophila* lacks FpoF, which is the subunit that accepts electrons from $F_{420}H_2$ in *Methanosarcina* species (23, 79). Rather, it has been proposed that iron clusters in the FpoB or FpoI subunits can accept electrons from reduced ferredoxin during acetoclastic growth, and heterodisulfide reduction was observed when *Mx. thermoacetophila* membranes were incubated with reduced ferredoxin from *Methanosarcina mazei* (21).

Another possibility is that a soluble iron-sulfur flavoprotein from the same family as FpoF (80, 81) interacts with the Fpo dehydrogenase complex to reduce $F_{420}$. The *Mx. thermoacetophila* genome has two genes (Mthe_0174 and Mthe_0959) from the FpoF family that code for proteins that are most similar to the beta subunit from the $F_{420}$ hydrogenase complex, FrhB. These proteins are not likely to be part of a hydrogenase complex, as the genome lacks genes that code for the other two subunits from this complex (FrhA and FrhG) (82), and hydrogenase activity has not been detected in *Mx. thermoacetophila* cells (21). One of these FrhB genes (Mthe_0174) was expressed at levels that were >6.6 times (*P* values $<2.6 \times 10^{-6}$) higher than the median RPKM values in all conditions (Table S3).

Reduced ferredoxin and/or $F_{420}H_2$ generated by Fpo dehydrogenase could then transfer electrons to either the soluble heterodisulfide reductase complex, HdrABC, or the membrane-bound heterodisulfide complex, HdrDE, to reduce CoM-S-S-CoB (Fig. 6). Levels of transcripts for *hdrA* (Mthe_1576) and *hdrDE* (Mthe_0980-0981) were >7.4 times (*P* values $<1.1 \times 10^{-6}$) and >5.0 times (*P* values $<2.7 \times 10^{-5}$) higher than the median RPKM values for all conditions (Table S3).

### Conclusions

*G. metallireducens* and *Mx. thermoacetophila* were able to grow syntrophically by coupling the oxidation of ethanol with the reduction of $CO_2$ to methane. Addition of the conductive material magnetite enhanced methanogenesis by acetate dismutation and by DIET, while GAC amendments impaired growth. Transcriptomic studies revealed that *G. metallireducens* uses mechanisms for electron transport to *Mx. thermoacetophila* that are similar to those used for electron transport to the type I *Methanosarcina*, *M. barkeri*. Both *M. barkeri* and *Mx. thermoacetophila* lack outer surface multiheme *c*-type cytochromes and putatively conductive archaella. Transcription of genes coding for gas vesicle proteins was downregulated during DIET or in the presence of magnetite likely because buoyancy within the water column is not required when cells can adhere to a surface. These results provide invaluable insight into *Methanothrix* physiology. However, further studies are required to fully understand the role of *Methanothrix* in methanogenic ecosystems.

## MATERIALS AND METHODS

### Culture conditions

*Mx. thermoacetophila* DSM 6194 was cultured anaerobically ($N_2/CO_2$ 80/20, v/v) at 55°C in DSMZ 334 medium (https://www.dsmz.de/microorganisms/medium/pdf/DSMZ_Medium334.pdf) with acetate (40 mM) as the substrate. *G. metallireducens* GS-15 (ATCC 53774) was routinely cultured anaerobically ($N_2/CO_2$ 80/20, v/v) at 30°C

in freshwater medium with ethanol (20 mM) as the electron donor and ferric citrate (56 mM) as the electron acceptor (83).

It was necessary to adapt both *G. metallireducens* and *Mx. thermoacetophila* to similar growth conditions before co-culture experiments could be conducted. *G. metallireducens* was adapted to grow in *Methanothrix* medium (DSMZ 334), in which acetate and sulfide were omitted, and ethanol (20 mM) and ferric citrate (56 mM) were supplied as the electron donor and the electron acceptor, respectively. The cultivation temperature for *G. metallireducens* was gradually increased from 30°C to 42°C, while the cultivation temperature for *Mx. thermoacetophila* was gradually decreased from 55°C to 42°C.

After *G. metallireducens* and *Mx. thermoacetophila* were adapted to grow at 42°C, an equal proportion (10%) of the two partners was added to modified DMSZ 334 medium with ethanol (20 mM) as the electron donor and $CO_2$ as the electron acceptor. Sulfide (0.5 mM) and L-cysteine·HCl (1 mM) were added from sterile anoxic stocks. The co-cultures were cultivated anaerobically ($N_2$/$CO_2$ 80/20, v/v) at 42°C.

When noted, GAC (Sigma-Aldrich, C2889, 8-20 mesh, various concentrations) or magnetite nanoparticles (10 mM) were added to the medium before autoclaving. The surface areas and resistivity of the GAC used was 600–800 $m^2$/g (dry basis) and 1,375 μΩ-cm (20°C), respectively. Magnetite nanoparticles with diameters of 20–50 nm were prepared as previously described (45).

## RNA extraction and transcriptome analyses

Triplicate cultures (co-cultures, pure cultures of *Mx. thermoacetophila* and pure cultures of *G. metallireducens*) were harvested during the midlogarithmic phase for transcriptomic analyses. Specifically, cells from co-cultures and pure cultures of *Mx. thermoacetophila* were collected when methane concentrations reached ~18 mM, and *G. metallireducens* cells were collected when Fe(II) concentrations were ~35 mM. Pellets from all samples were formed by centrifugation in 50 mL conical tubes at 4000×*g* for 15 min at 4°C. After centrifugation, the pellets were frozen in liquid nitrogen and stored at −80°C until RNA extraction procedures were performed.

Total RNA from sample pellets was extracted as previously described (84). Whole mRNAseq libraries were generated using the NEB Next UltraTM Directional RNA Library Prep Kit for Illumina (New England Biolabs, Ipswich, MA, USA). The clustering of index-coded samples was then performed on a cBot Cluster Generation System. After cluster generation, the library was sequenced on an Illumina Novaseq6000 platform and 150 bp paired-end reads were generated (Magigene Biotechnology, Guangzhou, China).

Raw data were checked with FASTQC (http://www.bioinformatics.babraham.ac.uk/projects/fastqc/), trimmed with Trimmomatic (85), and merged with FLASH (86). Ribosomal RNA (rRNA) reads were then removed from the libraries with SortMeRNA (87). The trimmed mRNA reads were mapped against genomes of *G. metallireducens* (CP000148) and *Mx. thermoacetophila* (CP000477) using SeqMan NGen (DNAStar). Reads were then normalized and processed for differential expression studies using the edgeR package in Bioconductor (88). All genes that were ≥1.5-fold differentially expressed with *P* values of ≤0.05 are reported in Supplementary Tables.

## DNA extraction and quantitative PCR

Genomic DNA was extracted from triplicate co-cultures with the MasterPure complete DNA purification kit (Lucigen). The proportion of *G. metallireducens* and *Mx. thermoacetophila* cells in co-cultures was determined with quantitative PCR using the following primer pairs: (i) Gm-f (5′-ATGGCCCACATCTTCATCTC-3′) and Gm-r (5′-TGCATGTTTTCATCCACGAT-3′) which amplified a 104-bp fragment from the *bamY* gene (Gmet_2143) encoding benzoate-CoA ligase of *G. metallireducens* (89), and (ii) Mx-f (5′-GAGGATCTTGCCCGGATATT-3′) and Mx-r (5′-TATTGTAACGCCAGAGCCTC-3′) which amplified a 102-bp fragment from the *sseA* gene (Mthe_1071) encoding the rhodanese domain protein of *Mx. thermoacetophila*. Quantitative PCR was performed with iTaq

Universal SYBR Green Supermix (Bio-Rad) on a QuantStudio 3 Real-Time PCR system (Applied Biosystems).

## Microscopy

Microbial cells were routinely checked with phase-contrast and fluorescence microscopy (Nikon E600) to ensure that cultures were not contaminated. Fluorescence *in situ* hybridization (FISH) of cell aggregates was conducted as previously described with a few modifications (90). Briefly, co-culture cells were fixed with 2% paraformaldehyde and 0.5% glutaraldehyde in 50 mM PIPES (pH 7.2) at 4°C for 2 h, followed by dehydration in 70% ethanol for 30 min. Cells were then transferred to glass slides, air dried, and immersed in hybridization buffer (900 mM NaCl, 20 mM Tris, 10% formamide, 0.01% SDS, 5 ng/μL each of the probes, pH 7.2) at 46°C for 2 h. Next, the slides were washed in washing buffer (450 mM NaCl, 20 mM Tris-HCl, 5 mM EDTA, 0.01% SDS, pH 7.2) at 48°C for 30 min, rinsed gently with Milli-Q water and examined with a laser scanning confocal microscope (Nikon Eclipse Ti2). Probes used in this study were MX825 (5′-[cy5]-TCGCACCGTGGCCGACACCTAGC) for *Mx. thermoacetophila* and Geo1 (5′-[cy3]-AGAATC-CAAGGACTCCGT) for *G. metallireducens* (4, 40, 91).

For negative-stained TEM, cells of *Mx. thermoacetophila* from either pure cultures or co-cultures were deposited on carbon-coated copper grids (200-mesh) for 10 min and stained with 2% phosphotungstic acid for 1 min. The grids were then air-dried and examined with a transmission electron microscope (ITACHI-HT7700) at 80 kV. For ultrathin TEM, the aggregates of co-cultures and pure cultures of *Mx. thermoacetophila* were fixed with 2% paraformaldehyde and 2.5% glutaraldehyde in 100 mM phosphate buffer (pH 7.2) at 4°C overnight and embedded in low-melt agarose (1.5% in phosphate buffer). The agarose-embedded aggregates were then fixed with 1% osmium tetroxide for 3 h, dehydrated in gradient ethanol solution (30%, 50%, 70%, 90%, 95%, and 100% two times), embedded in Spi-pon 812 resin, polymerized, sectioned, stained with lead citrate and examined with a transmission electron microscope (HITACHI-HT7800) at 80 kV.

For scanning electron microscopy, cells of *Mx. thermoacetophila* collected during the midlogarithmic phase were fixed with 2.5% glutaraldehyde in 100 mM phosphate buffer (pH 7.2) at 4°C overnight. Cells were then washed with phosphate buffer three times and post-fixed with 1% osmium tetroxide for 1 h. Fixed cells were dehydrated at 4°C with gradient ethanol solution (30%, 50%, 70%, 80%, 90%, 95%, and 100% two times) for 20 min for each step. Cells were then treated with ethanol/isoamyl acetate (v/v=1:1) for 30 min, and pure isoamyl acetate overnight. After dehydration, the samples were dried with a critical point dryer, coated with gold, and observed under a scanning electron microscope (HITACHI-SU8010) at 3 kV.

## Analytical techniques

Ethanol concentrations were measured with a gas chromatograph equipped with a flame ionization detector (Clarus 600; PerkinElmer Inc., San Jose, CA, USA). Acetate concentrations were measured by high-performance liquid chromatography (SHIMADZU, Japan) with an Aminex HPX-87H Ion Exclusion column (300 mm × 7.8 mm) and an eluent of 8.0 mM sulfuric acid. Methane was monitored by gas chromatography with a flame ionization detector (SHIMADZU, GC-8A) (92). Ferrous iron concentrations were determined by first incubating cultures in 0.5 N HCl and then measuring Fe(II) concentrations with a ferrozine assay at an absorbance of 562 nm as previously described (93).

## ACKNOWLEDGMENTS

We thank the Instrument Analysis Center of Shenzhen University for the assistance with the collection of transmission electron microscopy images.

This research was supported by the National Natural Science Foundation of China (42207144, 92251306, 32225003, and 31970105), the China Postdoctoral

Science Foundation (2021TQ0212), the Shenzhen Science and Technology Program (JCYJ20200109105010363), and the Innovation Team Project of Universities in Guangdong Province (2020KCXTD023).

The authors do not declare any conflicts of interest.

## AUTHOR AFFILIATIONS

[1]Archaeal Biology Center, Institute for Advanced Study, Shenzhen University, Shenzhen, Guangdong, China
[2]Laboratory of Optoelectronic Devices and Systems of Ministry of Education and Guangdong Province, College of Optoelectronic Engineering, Shenzhen University, Shenzhen, Guangdong, China
[3]Department of Microbiology, University of Massachusetts - Amherst, Amherst, Massachusetts, USA
[4]Shenzhen Key Laboratory of Marine Microbiome Engineering, Institute for Advanced Study, Shenzhen University, Shenzhen, Guangdong, China
[5]Department of Biomolecular Sciences, Central Connecticut State University, New Britain, Connecticut, USA
[6]Department of Physical and Biological Science, Western New England University, Springfield, Massachusetts, USA

## AUTHOR ORCIDs

Jessica A. Smith http://orcid.org/0000-0003-4248-6566
Meng Li http://orcid.org/0000-0001-8675-0758
Dawn E. Holmes http://orcid.org/0000-0002-1267-1771

## FUNDING


| Funder | Grant(s) | Author(s) |
|---|---|---|
| MOST \| National Natural Science Foundation of China (NSFC) | 42207144 | Jinjie Zhou |
| MOST \| National Natural Science Foundation of China (NSFC) | 92251306, 32225003, 31970105 | Meng Li |
| China Postdoctoral Science Foundation | 2021TQ0212 | Jinjie Zhou |
| Shenzhen Science and Technology Program | JCYJ20200109105010363 | Meng Li |
| Innovation Team Project of Universities in Guangdong Province | 2020KCXTD023 | Meng Li |


## AUTHOR CONTRIBUTIONS

Jinjie Zhou, Conceptualization, Data curation, Formal analysis, Funding acquisition, Investigation, Methodology, Validation, Visualization, Writing – original draft | Jessica A. Smith, Investigation, Visualization, Writing – review and editing | Meng Li, Funding acquisition, Project administration, Resources, Supervision, Validation, Writing – review and editing | Dawn E. Holmes, Conceptualization, Data curation, Investigation, Methodology, Resources, Software, Visualization, Writing – review and editing

## DATA AVAILABILITY STATEMENT

Illumina sequence reads have been submitted to the Sequence Read Archive (SRA) of the NCBI database under BioProject PRJNA914893 and Biosamples SAMN32360990, SAMN32360991, SAMN32360992, SAMN32360993, and SAMN32360994.

## ADDITIONAL FILES

The following material is available online.

### Supplemental Material

**Supplemental figures (mBio00360-23-s0001.pdf).** Figures S1 to S3.
**Table S1 (mBio00360-23-s0002.xlsx).** Genes that were differentially expressed by *G. metallireducens* grown under various conditions.
**Table S2 (mBio00360-23-s0003.xlsx).** Fold differences from median RPKM values for electron transport genes from *G. metallireducens* cells grown under various conditions.
**Table S3 (mBio00360-23-s0004.xlsx).** Fold difference from median RPKM values for *Mx. thermoacetophila* genes coding for surface proteins or proteins involved in carbon metabolism under various conditions.
**Table S4 (mBio00360-23-s0005.xlsx).** Genes that were differentially expressed by *Mx. thermoacetophila* grown under various conditions.
**Supplemental Text (mBio00360-23-s0006.pdf).** Carbon metabolism of *Mx. thermoacetophila* grown under various conditions.

## REFERENCES


1. Smith KS, Ingram-Smith C. 2007. *Methanosaeta*, the forgotten methanogen? Trends Microbiol 15:150–155. https://doi.org/10.1016/j.tim.2007.02.002
2. Holmes DE, Shrestha PM, Walker DJF, Dang Y, Nevin KP, Woodard TL, Lovley DR. 2017. Metatranscriptomic evidence for direct interspecies electron transfer between *Geobacter* and *Methanothrix* species in methanogenic rice paddy soils. Appl Environ Microbiol 83:e00223-17. https://doi.org/10.1128/AEM.00223-17
3. Großkopf R, Janssen PH, Liesack W. 1998. Diversity and structure of the methanogenic community in anoxic rice paddy soil microcosms as examined by cultivation and direct 16S rRNA gene sequence retrieval. Appl Environ Microbiol 64:960–969. https://doi.org/10.1128/AEM.64.3.960-969.1998
4. Rotaru A-E, Shrestha PM, Liu F, Shrestha M, Shrestha D, Embree M, Zengler K, Wardman C, Nevin KP, Lovley DR. 2014. A new model for electron flow during anaerobic digestion: direct interspecies electron transfer to *Methanosaeta* for the reduction of carbon dioxide to methane. Energy Environ Sci 7:408–415. https://doi.org/10.1039/C3EE42189A
5. Angle JC, Morin TH, Solden LM, Narrowe AB, Smith GJ, Borton MA, Rey-Sanchez C, Daly RA, Mirfenderesgi G, Hoyt DW, Riley WJ, Miller CS, Bohrer G, Wrighton KC. 2017. Methanogenesis in oxygenated soils is a substantial fraction of wetland methane emissions. Nat Commun 8:1567. https://doi.org/10.1038/s41467-017-01753-4
6. Tang Y, Shigematsu T, Morimura S, Kida K. 2005. Microbial community analysis of mesophilic anaerobic protein degradation process using bovine serum albumin (BSA) -fed continuous cultivation. J Biosci Bioeng 99:150–164. https://doi.org/10.1263/jbb.99.150
7. Díaz EE, Stams AJM, Amils R, Sanz JL. 2006. Phenotypic properties and microbial diversity of methanogenic granules from a full-scale upflow anaerobic sludge bed reactor treating brewery wastewater. Appl Environ Microbiol 72:4942–4949. https://doi.org/10.1128/AEM.02985-05
8. Morita M, Malvankar NS, Franks AE, Summers ZM, Giloteaux L, Rotaru AE, Rotaru C, Lovley DR. 2011. Potential for direct interspecies electron transfer in methanogenic wastewater digester aggregates. mBio 2:e00159–11. https://doi.org/10.1128/mBio.00159-11
9. Carr SA, Schubotz F, Dunbar RB, Mills CT, Dias R, Summons RE, Mandernack KW. 2018. Acetoclastic *Methanosaeta* are dominant methanogens in organic-rich Antarctic marine sediments. ISME J 12:330–342. https://doi.org/10.1038/ismej.2017.150
10. Tveit AT, Urich T, Frenzel P, Svenning MM. 2015. Metabolic and trophic interactions modulate methane production by Arctic peat microbiota in response to warming. Proc Natl Acad Sci U S A 112:E2507–E2516. https://doi.org/10.1073/pnas.1420797112
11. Romanowicz KJ, Crump BC, Kling GW. 2021. Rainfall alters permafrost soil redox conditions, but meta-omics show divergent microbial community responses by tundra type in the Arctic. Soil Syst 5:17. https://doi.org/10.3390/soilsystems5010017
12. Dean JF, Middelburg JJ, Röckmann T, Aerts R, Blauw LG, Egger M, Jetten MSM, de Jong AEE, Meisel OH, Rasigraf O, Slomp CP, in't Zandt MH, Dolman AJ. 2018. Methane feedbacks to the global climate system in a warmer world. Rev Geophys 56:207–250. https://doi.org/10.1002/2017RG000559
13. Rößger N, Sachs T, Wille C, Boike J, Kutzbach L. 2022. Seasonal increase of methane emissions linked to warming in Siberian tundra. Nat Clim Chang 12:1031–1036. https://doi.org/10.1038/s41558-022-01512-4
14. Meredith M, Sommerkorn M, Cassotta S, Derksen C, Ekaykin A, Hollowed A, Kofinas G, Mackintosh A, Melbourne-Thomas J, Muelbert M. 2019. Chapter 3, Polar regions. In IPCC special report on the ocean and Cryosphere in a changing climate. https://doi.org/10.1017/-9781009157964
15. Jetten MSM, Stams AJM, Zehnder AJB. 1992. Methanogenesis from acetate: a comparison of the acetate metabolism in *Methanothrix soehngenii* and *Methanosarcina* spp. FEMS Microbiol Rev 88:181–198. https://doi.org/10.1111/j.1574-6968.1992.tb04987.x
16. Ferry JG. 2010. How to make a living by exhaling methane. Annu Rev Microbiol 64:453–473. https://doi.org/10.1146/annurev.micro.112408.134051
17. Sun H, Angelidaki I, Wu S, Dong R, Zhang Y. 2018. The potential of bioelectrochemical sensor for monitoring of acetate during anaerobic digestion: focusing on novel reactor design. Front Microbiol 9:3357. https://doi.org/10.3389/fmicb.2018.03357
18. Pan X, Zhao L, Li C, Angelidaki I, Lv N, Ning J, Cai G, Zhu G. 2021. Deep insights into the network of acetate metabolism in anaerobic digestion: focusing on syntrophic acetate oxidation and homoacetogenesis. Water Res 190:116774. https://doi.org/10.1016/j.watres.2020.116774
19. Yee MO, Rotaru AE. 2020. Extracellular electron uptake in *Methanosarcinales* is independent of multiheme *c*-type cytochromes. Sci Rep 10:372. https://doi.org/10.1038/s41598-019-57206-z
20. Stams AJM, Teusink B, Sousa DZ. 2019. Ecophysiology of Acetoclastic Methanogens, p 1–14. In Stams AJM, DZ Sousa (ed), Biogenesis of hydrocarbons. Springer International Publishing, Cham. https://doi.org/10.1007/978-3-319-53114-4
21. Welte C, Deppenmeier U. 2011. Membrane-bound electron transport in *Methanosaeta thermophila*. J Bacteriol 193:2868–2870. https://doi.org/10.1128/JB.00162-11
22. Berger S, Welte C, Deppenmeier U. 2012. Acetate activation in *Methanosaeta thermophila*: characterization of the key enzymes pyrophosphatase and acetyl-CoA synthetase. Archaea 2012:315153. https://doi.org/10.1155/2012/315153

23. Welte C, Deppenmeier U. 2014. Bioenergetics and anaerobic respiratory chains of aceticlastic methanogens. Biochim Biophys Acta 1837:1130–1147. https://doi.org/10.1016/j.bbabio.2013.12.002
24. Huang Y, Cai B, Dong H, Li H, Yuan J, Xu H, Wu H, Xu Z, Sun D, Dang Y, Holmes DE. 2022. Enhancing anaerobic digestion of food waste with granular activated carbon immobilized with riboflavin. Sci Total Environ 851:158172. https://doi.org/10.1016/j.scitotenv.2022.158172
25. Liu C, Sun D, Zhao Z, Dang Y, Holmes DE. 2019. *Methanothrix* enhances biogas upgrading in microbial electrolysis cell via direct electron transfer. Bioresour Technol 291:121877. https://doi.org/10.1016/j.biortech.2019.121877
26. Liu C, Yuan X, Gu Y, Chen H, Sun D, Li P, Li M, Dang Y, Smith JA, Holmes DE. 2020. Enhancement of bioelectrochemical $CO_2$ reduction with a carbon brush electrode via direct electron transfer. ACS Sust Chem Eng 8:11368–11375. https://doi.org/10.1021/acssuschemeng.0c03623
27. Holmes DE, Rotaru A-E, Ueki T, Shrestha PM, Ferry JG, Lovley DR. 2018. Electron and proton flux for carbon dioxide reduction in *Methanosarcina barkeri* during direct interspecies electron transfer. Front Microbiol 9:3109. https://doi.org/10.3389/fmicb.2018.03109
28. Holmes DE, Zhou J, Ueki T, Woodard T, Lovley DR. 2021. Mechanisms for electron uptake by *Methanosarcina acetivorans* during direct interspecies electron transfer. mBio 12:e0234421. https://doi.org/10.1128/mBio.02344-21
29. Huang L, Liu X, Zhang Z, Ye J, Rensing C, Zhou S, Nealson KH. 2022. Light-driven carbon dioxide reduction to methane by *Methanosarcina barkeri* in an electric syntrophic coculture. ISME J 16:370–377. https://doi.org/10.1038/s41396-021-01078-7
30. Conklin A, Stensel HD, Ferguson J. 2006. Growth kinetics and competition between *Methanosarcina* and *Methanosaeta* in mesophilic anaerobic digestion. Water Environ Res 78:486–496. https://doi.org/10.2175/106143006x95393
31. Yang P, Tan G-YA, Aslam M, Kim J, Lee P-H. 2019. Metatranscriptomic evidence for classical and RuBisCo-mediated $CO_2$ reduction to methane facilitated by direct interspecies electron transfer in a methanogenic system. Sci Rep 9:4116. https://doi.org/10.1038/s41598-019-40830-0
32. Kono T, Mehrotra S, Endo C, Kizu N, Matusda M, Kimura H, Mizohata E, Inoue T, Hasunuma T, Yokota A, Matsumura H, Ashida H. 2017. A RuBisCO-mediated carbon metabolic pathway in methanogenic archaea. Nat Commun 8:14007. https://doi.org/10.1038/ncomms14007
33. Xiao L, Lichtfouse E, Senthil Kumar P. 2021. Advantage of conductive materials on interspecies electron transfer-independent acetoclastic methanogenesis: a critical review. Fuel 305:121577. https://doi.org/10.1016/j.fuel.2021.121577
34. Zhao Z, Li Y, Zhang Y, Lovley DR. 2020. Sparking anaerobic digestion: promoting direct interspecies electron transfer to enhance methane production. iScience 23:101794. https://doi.org/10.1016/j.isci.2020.101794
35. Rotaru AE, Shrestha PM, Liu F, Markovaite B, Chen S, Nevin KP, Lovley DR. 2014. Direct interspecies electron transfer between *Geobacter metallireducens* and *Methanosarcina barkeri*. Appl Environ Microbiol 80:4599–4605. https://doi.org/10.1128/AEM.00895-14
36. Chen S, Rotaru A-E, Liu F, Philips J, Woodard TL, Nevin KP, Lovley DR. 2014. Carbon cloth stimulates direct interspecies electron transfer in syntrophic co-cultures. Bioresour Technol 173:82–86. https://doi.org/10.1016/j.biortech.2014.09.009
37. Zheng S, Liu F, Wang B, Zhang Y, Lovley DR. 2020. *Methanobacterium* capable of direct interspecies electron transfer. Environ Sci Technol 54:15347–15354. https://doi.org/10.1021/acs.est.0c05525
38. Liu F, Rotaru A-E, Shrestha PM, Malvankar NS, Nevin KP, Lovley DR. 2012. Promoting direct interspecies electron transfer with activated carbon. Energy Environ. Sci 5:8982. https://doi.org/10.1039/c2ee22459c
39. Shrestha PM, Rotaru AE, Summers ZM, Shrestha M, Liu F, Lovley DR. 2013. Transcriptomic and genetic analysis of direct interspecies electron transfer. Appl Environ Microbiol 79:2397–2404. https://doi.org/10.1128/AEM.03837-12
40. Summers ZM, Fogarty HE, Leang C, Franks AE, Malvankar NS, Lovley DR. 2010. Direct exchange of electrons within aggregates of an evolved syntrophic coculture of anaerobic bacteria. Science 330:1413–1415. https://doi.org/10.1126/science.1196526
41. Kamagata Y, Mikami E. 1991. Isolation and characterization of a novel thermophilic *Methanosaeta* strain. Int J Syst Evol Microbiol 41:191–196. https://doi.org/10.1099/00207713-41-2-191
42. Zhou J, Holmes DE, Tang H-Y, Lovley DR. 2021. Correlation of key physiological properties of *Methanosarcina* isolates with environment of origin. Appl Environ Microbiol 87:e0073121. https://doi.org/10.1128/AEM.00731-21
43. Shrestha PM, Rotaru AE, Aklujkar M, Liu F, Shrestha M, Summers ZM, Malvankar N, Flores DC, Lovley DR. 2013. Syntrophic growth with direct interspecies electron transfer as the primary mechanism for energy exchange. Environ Microbiol Rep 5:904–910. https://doi.org/10.1111/1758-2229.12093
44. Yee MO, Snoeyenbos-West OL, Thamdrup B, Ottosen LDM, Rotaru AE. 2019. Extracellular electron uptake by two *Methanosarcina* species. Front Energy Res 7:29. https://doi.org/10.3389/fenrg.2019.00029
45. Liu F, Rotaru AE, Shrestha PM, Malvankar NS, Nevin KP, Lovley DR. 2015. Magnetite compensates for the lack of a pilin-associated *c*-type cytochrome in extracellular electron exchange. Environ Microbiol 17:648–655. https://doi.org/10.1111/1462-2920.12485
46. Rotaru A-E, Calabrese F, Stryhanyuk H, Musat F, Shrestha PM, Weber HS, Snoeyenbos-West OLO, Hall POJ, Richnow HH, Musat N, Thamdrup B. 2018. Conductive particles enable sntrophic acetate oxidation between *Geobacter* and *Methanosarcina* from coastal sediments. mBio 9:e00226-18. https://doi.org/10.1128/mBio.00226-18
47. Maher BA, Taylor RM. 1988. Formation of ultrafine-grained magnetite in soils. Nature 336:368–370. https://doi.org/10.1038/336368a0
48. Abbas Y, Yun S, Wang Z, Zhang Y, Zhang X, Wang K. 2021. Recent advances in bio-based carbon materials for anaerobic digestion: a review. Renew Sust Energ Rev 135:110378. https://doi.org/10.1016/j.rser.2020.110378
49. Park JH, Kang HJ, Park KH, Park HD. 2018. Direct interspecies electron transfer via conductive materials: a perspective for anaerobic digestion applications. Bioresour Technol 254:300–311. https://doi.org/10.1016/j.biortech.2018.01.095
50. Yu N, Guo B, Zhang Y, Zhang L, Zhou Y, Liu Y. 2021. Self-fluidized GAC-amended UASB reactor for enhanced methane production. Chem Eng J 420:127652. https://doi.org/10.1016/j.cej.2020.127652
51. Xu S, He C, Luo L, Lü F, He P, Cui L. 2015. Comparing activated carbon of different particle sizes on enhancing methane generation in upflow anaerobic digester. Bioresour Technol 196:606–612. https://doi.org/10.1016/j.biortech.2015.08.018
52. Dang Y, Sun D, Woodard TL, Wang LY, Nevin KP, Holmes DE. 2017. Stimulation of the anaerobic digestion of the dry organic fraction of municipal solid waste (OFMSW) with carbon-based conductive materials. Bioresour Technol 238:30–38. https://doi.org/10.1016/j.biortech.2017.04.021
53. Lei Y, Sun D, Dang Y, Feng X, Huo D, Liu C, Zheng K, Holmes DE. 2019. Metagenomic analysis reveals that activated carbon aids anaerobic digestion of raw incineration leachate by promoting direct interspecies electron transfer. Water Res 161:570–580. https://doi.org/10.1016/j.watres.2019.06.038
54. Fu L, Zhou T, Wang J, You L, Lu Y, Yu L, Zhou S. 2019. Nano$Fe_3O_4$ as solid electron shuttles to accelerate acetotrophic methanogenesis by *Methanosarcina barkeri*. Front Microbiol 10:388. https://doi.org/10.3389/fmicb.2019.00388
55. Wang H, Byrne JM, Liu P, Liu J, Dong X, Lu Y. 2020. Redox cycling of Fe (II) and Fe (III) in magnetite accelerates aceticlastic methanogenesis by *Methanosarcina mazei*. Environ Microbiol Rep 12:97–109. https://doi.org/10.1111/1758-2229.12819
56. Lei Y, Wei L, Liu T, Xiao Y, Dang Y, Sun D, Holmes DE. 2018. Magnetite enhances anaerobic digestion and methanogenesis of fresh leachate from a municipal solid waste incineration plant. Chem Eng J 348:992–999. https://doi.org/10.1016/j.cej.2018.05.060
57. Kato S, Hashimoto K, Watanabe K. 2012. Methanogenesis facilitated by electric syntrophy via (semi) conductive iron-oxide minerals. Environ Microbiol 14:1646–1654. https://doi.org/10.1111/j.1462-2920.2011.02611.x
58. Holmes DE, Zhou J, Smith JA, Wang C, Liu X, Lovley DR. 2022. Different outer membrane *c* - type cytochromes are involved in direct interspecies electron transfer to *Geobacter* or *Methanosarcina* species. mLife 1:272–286. https://doi.org/10.1002/mlf2.12037

59. Shi L, Dong H, Reguera G, Beyenal H, Lu A, Liu J, Yu HQ, Fredrickson JK. 2016. Extracellular electron transfer mechanisms between microorganisms and minerals. Nat Rev Microbiol 14:651–662. https://doi.org/10.1038/nrmicro.2016.93
60. Ueki T. 2021. Cytochromes in extracellular electron transfer in *Geobacter*. Appl Environ Microbiol 87:e03109-20. https://doi.org/10.1128/AEM.03109-20
61. Shi L, Fredrickson JK, Zachara JM. 2014. Genomic analyses of bacterial porin-cytochrome gene clusters. Front Microbiol 5:657. https://doi.org/10.3389/fmicb.2014.00657
62. Reguera G, McCarthy KD, Mehta T, Nicoll JS, Tuominen MT, Lovley DR. 2005. Extracellular electron transfer via microbial nanowires. Nature 435:1098–1101. https://doi.org/10.1038/nature03661
63. Liu X, Zhan J, Jing X, Zhou S, Lovley DR. 2019. A pilin chaperone required for the expression of electrically conductive *Geobacter sulfurreducens* pili . Environ Microbiol 21:2511–2522. https://doi.org/10.1111/1462-2920.14638
64. Zheng S, Liu F. 2021. Complete genome sequence of *Methanobacterium electrotrophus* strain YSL, isolated from coastal riverine sediments. Microbiol Resour Announc 10:e0075221. https://doi.org/10.1128/MRA.00752-21
65. Ueki T, Nevin KP, Rotaru A-E, Wang L-Y, Ward JE, Woodard TL, Lovley DR. 2018. *Geobacter* strains expressing poorly conductive pili reveal constraints on direct interspecies electron transfer mechanisms. mBio 9:e01273-18. https://doi.org/10.1128/mBio.01273-18
66. Butler JE, Young ND, Lovley DR. 2010. Evolution of electron transfer out of the cell: comparative genomics of six *Geobacter* genomes. BMC Genomics 11:40. https://doi.org/10.1186/1471-2164-11-40
67. Zhong Y, Shi L. 2018. Genomic analyses of the quinol oxidases and/or quinone reductases involved in bacterial extracellular electron transfer. Front Microbiol 9:3029. https://doi.org/10.3389/fmicb.2018.03029
68. Smith JA, Lovley DR, Tremblay PL. 2013. Outer cell surface components essential for Fe (III) oxide reduction by *Geobacter metallireducens*. Appl Environ Microbiol 79:901–907. https://doi.org/10.1128/AEM.02954-12
69. Lloyd JR, Leang C, Myerson ALH, Coppi MV, Cuifo S, Methe B, Sandler SJ, Lovley DR. 2003. Biochemical and genetic characterization of PpcA, a periplasmic *c*-type cytochrome in *Geobacter sulfurreducens*. Biochem J 369:153–161. https://doi.org/10.1042/bj20020597
70. Morgado L, Dantas JM, Bruix M, Londer YY, Salgueiro CA. 2012. Fine tuning of redox networks on multiheme cytochromes from *Geobacter sulfurreducens* drives physiological electron/proton energy transduction. Bioinorg Chem Appl 2012:298739. https://doi.org/10.1155/2012/298739
71. Dueholm MS, Larsen P, Finster K, Stenvang MR, Christiansen G, Vad BS, Bøggild A, Otzen DE, Nielsen PH. 2015. The tubular sheaths encasing *Methanosaeta thermophila* filaments are functional amyloids. J Biol Chem 290:20590–20600. https://doi.org/10.1074/jbc.M115.654780
72. Pfeifer F. 2012. Distribution, formation and regulation of gas vesicles. Nat Rev Microbiol 10:705–715. https://doi.org/10.1038/nrmicro2834
73. Shipps C, Kelly HR, Dahl PJ, Yi SM, Vu D, Boyer D, Glynn C, Sawaya MR, Eisenberg D, Batista VS, Malvankar NS. 2021. Intrinsic electronic conductivity of individual atomically resolved amyloid crystals reveals micrometer-long hole hopping via tyrosines. Proc Natl Acad Sci U S A 118:e2014139118. https://doi.org/10.1073/pnas.2014139118
74. Lovley DR, Ueki T, Zhang T, Malvankar NS, Shrestha PM, Flanagan KA, Aklujkar M, Butler JE, Giloteaux L, Rotaru A-E, Holmes DE, Franks AE, Orellana R, Risso C, Nevin KP. 2011. *Geobacter*: the microbe electric's physiology, ecology, and practical applications, p 1–100. In Poole RK (ed), Advances in microbial physiology. Academic Press.
75. Lovley DR, Holmes DE. 2022. Electromicrobiology: the ecophysiology of phylogenetically diverse electroactive microorganisms. Nat Rev Microbiol 20:5–19. https://doi.org/10.1038/s41579-021-00597-6
76. Barber RD, Zhang L, Harnack M, Olson MV, Kaul R, Ingram-Smith C, Smith KS. 2011. Complete genome sequence of *Methanosaeta concilii*, a specialist in aceticlastic methanogenesis. J Bacteriol 193:3668–3669. https://doi.org/10.1128/JB.05031-11
77. Pons T, Gómez R, Chinea G, Valencia A. 2003. Beta-propellers: associated functions and their role in human diseases. Curr Med Chem 10:505–524. https://doi.org/10.2174/0929867033368204
78. Kopec KO, Lupas AN. 2013. β-propeller blades as ancestral peptides in protein evolution. PLoS One 8:e77074. https://doi.org/10.1371/journal.pone.0077074
79. Welte C, Deppenmeier U. 2011. Re-evaluation of the function of the $F_{420}$ dehydrogenase in electron transport of *Methanosarcina mazei*. FEBS J 278:1277–1287. https://doi.org/10.1111/j.1742-4658.2011.08048.x
80. Johnson EF, Mukhopadhyay B. 2005. A new type of sulfite reductase, a novel coenzyme $F_{420}$-dependent enzyme, from the methanarchaeon *Methanocaldococcus jannaschii*. J Biol Chem 280:38776–38786. https://doi.org/10.1074/jbc.M503492200
81. Mills DJ, Vitt S, Strauss M, Shima S, Vonck J. 2013. De novo modeling of the $F_{420}$-reducing [Nife]-hydrogenase from a methanogenic archaeon by cryo-electron microscopy. Elife 2:e00218. https://doi.org/10.7554/eLife.00218
82. Kulkarni G, Mand TD, Metcalf WW. 2018. Energy conservation via hydrogen cycling in the methanogenic archaeon *Methanosarcina barkeri*. mBio 9:e01256-18. https://doi.org/10.1128/mBio.01256-18
83. Lovley DR, Giovannoni SJ, White DC, Champine JE, Phillips EJ, Gorby YA, Goodwin S. 1993. *Geobacter metallireducens* gen. nov. sp. nov., a microorganism capable of coupling the complete oxidation of organic compounds to the reduction of iron and other metals. Arch Microbiol 159:336–344. https://doi.org/10.1007/BF00290916
84. Holmes DE, Risso C, Smith JA, Lovley DR. 2012. Genome-scale analysis of anaerobic benzoate and phenol metabolism in the hyperthermophilic archaeon *Ferroglobus placidus*. ISME J 6:146–157. https://doi.org/10.1038/ismej.2011.88
85. Bolger AM, Lohse M, Usadel B. 2014. Trimmomatic: a flexible trimmer for Illumina sequence data. Bioinformatics 30:2114–2120. https://doi.org/10.1093/bioinformatics/btu170
86. Magoč T, Salzberg SL. 2011. FLASH: fast length adjustment of short reads to improve genome assemblies. Bioinformatics 27:2957–2963. https://doi.org/10.1093/bioinformatics/btr507
87. Kopylova E, Noé L, Touzet H. 2012. SortMeRNA: fast and accurate filtering of ribosomal RNAs in metatranscriptomic data. Bioinformatics 28:3211–3217. https://doi.org/10.1093/bioinformatics/bts611
88. Robinson MD, McCarthy DJ, Smyth GK. 2010. edgeR: a Bioconductor package for differential expression analysis of digital gene expression data. Bioinformatics 26:139–140. https://doi.org/10.1093/bioinformatics/btp616
89. Smith JA, Nevin KP, Lovley DR. 2015. Syntrophic growth via quinone-mediated interspecies electron transfer. Front Microbiol 6:121. https://doi.org/10.3389/fmicb.2015.00121
90. Pernthaler J, Glöckner F-O, Schönhuber W, Amann R. 2001. Fluorescence *in situ* hybridization (FISH) with rRNA-targeted oligonucleotide probes. Methods Microbiol 30:207–226. https://doi.org/10.1016/S0580-9517(01)30046-6
91. Raskin L, Stromley JM, Rittmann BE, Stahl DA. 1994. Group-specific 16S rRNA hybridization probes to describe natural communities of methanogens. Appl Environ Microbiol 60:1232–1240. https://doi.org/10.1128/aem.60.4.1232-1240.1994
92. Holmes DE, Giloteaux L, Orellana R, Williams KH, Robbins MJ, Lovley DR. 2014. Methane production from protozoan endosymbionts following stimulation of microbial metabolism within subsurface sediments. Front Microbiol 5:366. https://doi.org/10.3389/fmicb.2014.00366
93. Lovley DR, Phillips EJ. 1986. Organic matter mineralization with reduction of ferric iron in anaerobic sediments. Appl Environ Microbiol 51:683–689. https://doi.org/10.1128/aem.51.4.683-689.1986